Int. J. Electrochem. Sci., 10 **(2015)** 9824 - 9836

International Journal of
ELECTROCHEMICAL
SCIENCE
www.electrochemsci.org

Preparation of RuO_2/Nano-Graphite Cathode for Electrocatalytic Degradation of Phenol

Na Wang [1], *Dong Li* [1], *Li Yu* [1], *Xiujuan Yu* [1,*], *Tianyi Sun* [2]

[1] Department of Environmental Science and Engineering, Heilongjiang University, Harbin, 150080, PR China
[2] State Key Laboratory of Urban Water Resource and Environment, Harbin Institute of Technology, Harbin 150090, PR China
[*]E-mail: yuxiujuan@hlju.edu.cn

Received: 26 May 2015 / *Accepted:* 22 September 2015 / *Published:* 4 November 2015

A RuO_2/nano-graphite composite was prepared by the chemical precipitation strategy. The as-prepared samples were characterized by SEM, XRD, XPS, AFM and Raman spectroscopy. RuO_2 with a mixture of amorphous hydrous and crystalline states was found on the surface of nano-graphite. RuO_2/nano-graphite, used as the cathode in a diaphragm cell with a Ti/IrO_2/RuO_2 anode, exhibited enhanced catalytic activity in the electro-oxidation degradation of phenol. After 120 min electrolysis, the removal efficiencies of phenol (100 mg/L) and COD (1200 mg/L) reached 95.3% and 88.6%, respectively. RuO_2 could improve the generation of H_2O_2 by O_2 reduction and accelerate the production of •OH from the decomposition of H_2O_2.

Keywords: RuO_2, Nano-graphite, Electrocatalysis, Cathode

1. INTRODUCTION

The removal of pollutants by using electrochemical catalytic oxidation technology could be conducted via cathode reduction [1-4]. To improve the removal efficiency of the pollutant and save electric energy, more and more researchers are focusing on the degradation of organic pollutants by the synergetic electro-catalytic effects of direct anodic oxidation and indirect cathodic reduction [5], which can effectively maintain the superiority of the anodic oxidation and simultaneously eliminate the organic pollutants due to the strong active species from the cathode reduction reaction of O_2, such as H_2O_2, HO_2^-, HO• and HO_2•[6,7].

Among the many anode materials, dimensionally stable anodes (DSA), such as Ti/RuO_2 and PbO_2, are subjects of particular interest[8-11]. Cathode materials such as activated carbon[12-14],

carbon fibre[15], carbon sponge[16] and graphite[17-19] were studied for the removal of organics by synergetic degradation. Li Fan [5] has studied the degradation of amaranth under the galvanostatic model, and activated carbon fibres were simultaneously used as the anode and the cathode. As much as 99% of colour could be degraded at a current density of 0.50 $mA \cdot cm^{-2}$. The degradation of phenol was studied in a novel electrocatalytic system with graphite as the cathode and TiO_2/activated carbon fibre as the anode by Peipei Jin[17]. With the formation of hydroxyl radicals, phenol was oxidized to hydroquinone, pyrocatechol and benzoquinone during the electrocatalytic process. Then, these intermediate products gradually diminished and were degraded to form opened products such as formic and maleic acids, which were ultimately oxidized to CO_2 and H_2O. Additionally, the degradation of 4-nitrophenol was investigated by Y.Y. Chu[18] using a novel electrochemical oxidation system with two cathodes, where the gas diffusion electrode was used to generate H_2O_2 by O_2 reduction, and the graphite cathode was employed for the reduction of Fe^{3+}, regenerating Fe^{2+}. Due to the combination of cathodic reduction and anodic oxidation, effective degradation was achieved.

Recently, two-dimensional (2D) nano-architectures, such as nano-graphite, have been considered as a versatile candidate for the improvement of electrocatalytic performance thanks to the outstanding charge-transport and accelerating the two-electron reduction of O_2 to H_2O_2. In addition, nano-graphite can be fabricated on a large scale compared to its counterparts [4]. In this work, a new supported catalyst constructed by coupling the RuO_2 nano-crystals uniformly on the nano-graphite was synthesized via a precipitation strategy. RuO_2/nano-graphite was used as the cathode to improve the phenol degradation efficiency of the indirect cathodic oxidation by accelerating the yield of hydrogen peroxide and free radical. The morphological characteristics and constituents of the resulting RuO_2/nano-graphite composite were analyzed by SEM, XRD, XPS and Raman spectroscopy. In addition, the thicknesses of nano-graphite and RuO_2/nano-graphite flake were accurately confirmed through AFM measurement. The catalytic action of the RuO_2/nano-graphite cathode was evaluated by the removal of phenol and its COD. Finally, the enhanced electrocatalytic mechanism was discussed in detail by detecting and analyzing the concentration of H_2O_2 produced at the RuO_2/nano-graphite cathode and the generation of •OH derived from the decomposition of H_2O_2. As a result, the RuO_2/nano-graphite composite cathode exhibited superior electrocatalytic performance.

2. EXPERIMENTAL

2.1. Experimental materials

Natural flake graphite (carbon content, 95 wt.%), perchloric acid (72 wt.%; A.R.), ethyl alcohol (99.7 wt.%; A.R.), ruthenium trichloride(Ru,36.7%) and ammonia water(28 wt.%, A.R.) were purchased from Sinopharm Chemical Reagent Co., Ltd.. All chemicals used in our study were analytical grade and employed without further purification, and distilled (DI) water was used throughout all our experiments.

2.2. Synthesis and characterizatin of RuO_2/nano-graphite

Nano-graphite was prepared according to our previous study [4]. RuO_2/nano-graphite composite catalyst was prepared by the precipitation method and calcination. The desired amount of nano-graphite was introduced into the distilled water and stirred for a few minutes. Subsequently, 25 mL of 0.01 mol/L ruthenium chloride solution and the same volume of ammonium hydroxide were added dropwise into the nano-graphite. The obtained solution was mixed under vigorous stirring for 30 min at 65 °C. Afterwards the wet precipitate was dried in an oven at 100 °C for 12 h. Then, the black powders were calcinated in a muffle furnace for 3 h at 300 °C. Finally, RuO_2/nano-graphite was obtained.

The structural and morphological characterizations of the catalyst were performed by a variety of surface science techniques such as SEM (Hitachi S4800) with energy dispersive X-ray spectroscopy (EDS), AFM (SPM 5100 atomic force microscope measurements were conducted in the tapping mode), XPS (PHI 5700), XRD (D/max-ⅢB) and Raman spectroscopy (HR800JY in France).

2.3. Preparation of the cathode

The RuO_2/nano-graphite and pure nano-graphite were placed in a beaker with 3.0 mL ethanol as a dispersant and 4 g diluted PFTE latex (10 wt%) as a binder and fixed in a water bath in order to obtain a paste. The paste was then rolled on the stainless steel mesh by a presser. The resulting RuO_2/nano-graphite was cut into 4 cm×4 cm pieces as the cathode. In a typical procedure, RuO_2/nano-graphite cathodes containing 2%, 4% and 6% ruthenium were prepared.

2.4. The electrocatalytic performance evaluation of the cathode

The electrocatalytic performance of the cathode was evaluated by the removal of phenol and the chemical oxygen demand (COD) in the cathode apartment. The electrocatalytic degradations were conducted in a self-made terylene diaphragm cell with a volume of 150 mL, which was constructed by assembling two equal size electrodes with internal dimensions of 4 cm × 4 cm. Ti/IrO_2/RuO_2 net and the as-prepared RuO_2/nano-graphite electrode were used as the anode and cathode, respectively. The anode and cathode were fixed parallel to each other with an inner gap of 3 cm. The simulated wastewater was prepared by dissolving phenol to 100 mg/L in distilled water, and its conductivity was raised by adding Na_2SO_4 (0.1 mol/L). The concentration of phenol was measured using a UV-vis spectrophotometer at a wavelength of 510 nm by the 4-aminoantipyrine method.

To understand the degradation mechanism of the organic pollutant by the RuO_2/nano-graphite cathode, the generation of hydrogen peroxide (H_2O_2) and hydroxyl radicals (•OH) was measured. The H_2O_2 concentration accumulated during electrolysis was determined by titration with permanganate using a standard procedure [20]. The production of •OH radicals at the prepared cathode/water interface was detected by measuring the fluorescence (FL, RF-5301PC) spectra derived from the reaction with terephthalic acid (TA), which could readily react with the generated •OH to form a highly fluorescent product, 2-hydroxyterephthalia acid(TAOH).

3. RESULTS AND DISCUSSION

3.1. SEM and EDS

SEM micrographs of nano-graphite and RuO_2/nano-graphite are showed in Fig. 1. The nano-graphite in Fig. 1a and Fig. 1b exhibited a lamellate shape, some of which was clearly crackled. The nano-graphite in the RuO_2/nano-graphite (Fig. 1b) also kept its flake-like structure and was not significantly different from its initial state in shape. This result indicated that the modified process with RuO_2 did not alter the flake structure of the nano-graphite.

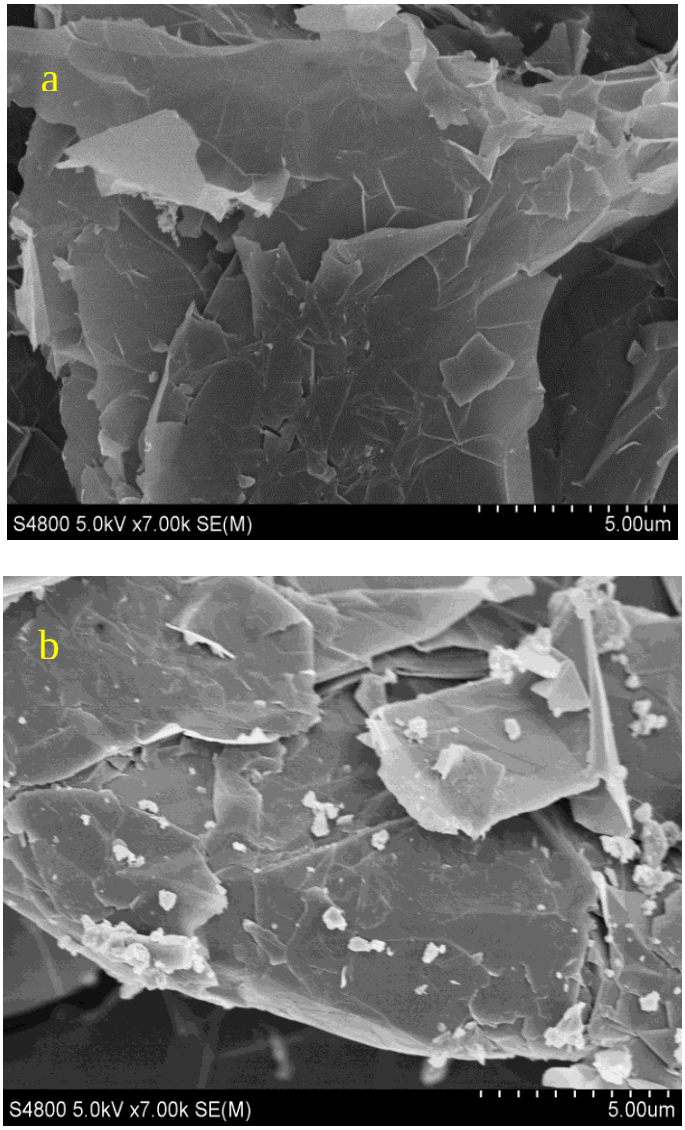

Figure 1. SEM image of nano-graphite (a) and RuO_2/nano-graphite (b)

The corresponding EDS spectrum of RuO_x/nano-graphite is displayed in Fig. 2, demonstrating the presence of C, Ru, and O. The EDS and SEM spectra suggested that Ru was uniformly deposited on the nano-graphite surface.

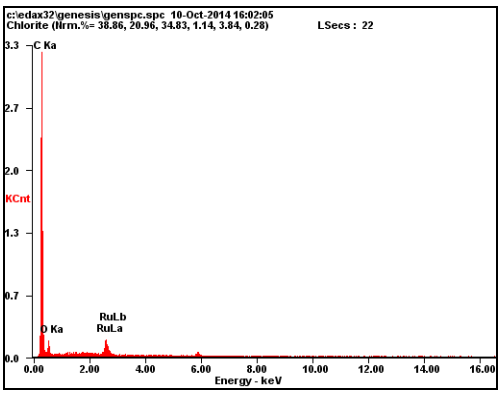

Figure 2. EDS spectra of RuO_2/nano-graphite

3.2. XPS and XRD

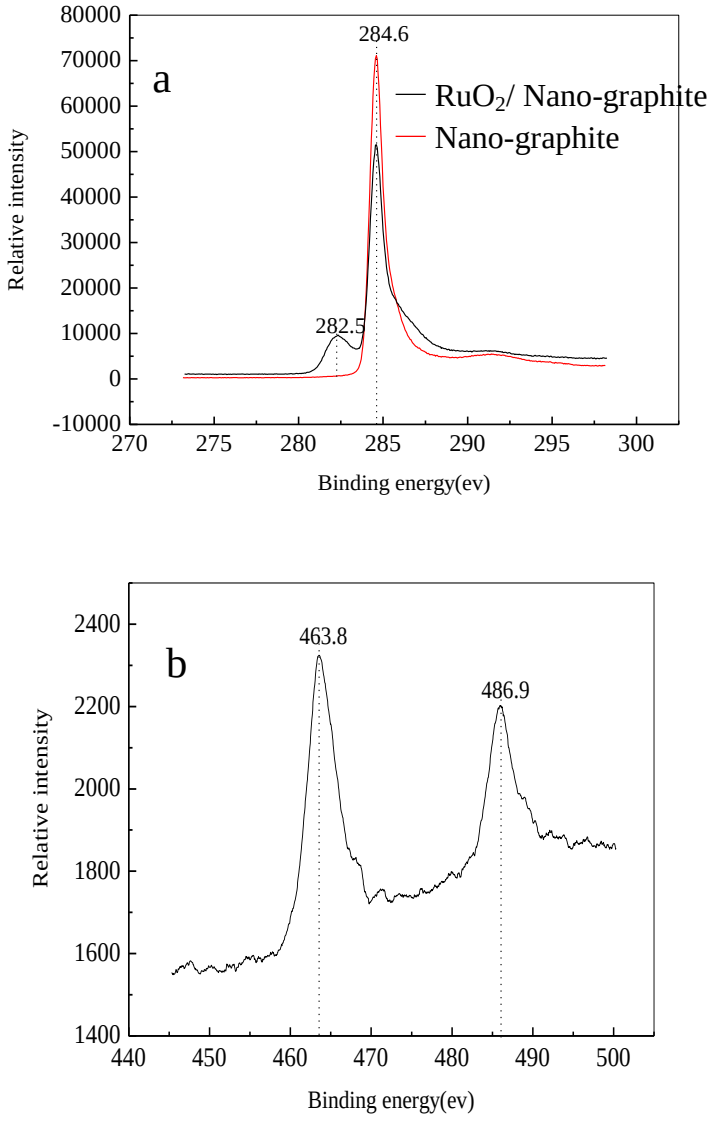

Figure 3. XPS spectrum of Ru3d (a) and Ru3p (b) in RuO_2/nano-graphite sample

XPS can provide powerful information regarding the chemical state of a sample [21]. The XPS spectra of RuO_x/nano-graphite are plotted in Fig. 3. There are two characteristic peaks in XPS spectrum of RuO_2/nano-graphite. One peak could be clearly observed at 282.5 eV, belonging to the Ru3d5/2 corresponding to the Ru3d of the hydrated RuO_2[22].

The other peak was located at 284.6eV, as shown in Fig. 3a, and is the C 1s peak from nano-graphite. With the introduction of ruthenium, the C 1s peak of the RuO_2/nano-graphite became lower, indicating that RuO_2 was evenly dispersed on the surface of nano-graphite. Because the C 1s peak of the nano-graphite and the Ru 3d3/2 peak overlap each other, the Ru 3p spectrum was also used to determine the presence of oxidation states of Ru species (Fig. 3b)[23]. The Ru3p spectrum of RuO_x/nano-graphite is shown in Fig. 3b. Two broad peaks are visible at 463.8 eV and 486.9 eV, which can be ascribed to the presence of hydrous amorphous $RuO_2 \cdot xH_2O$ [24,25].

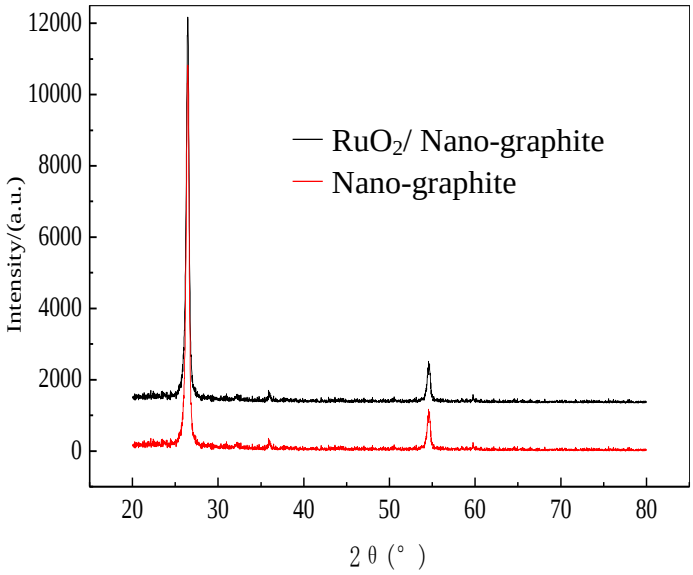

Figure 4. XRD spectra of nano-graphite and RuO_2/nano-graphite

Fig. 4 shows the XRD patterns of nano-graphite and RuO_2/nano-graphite. In Fig. 4, the relatively broad diffraction peak observed at $2\theta \approx 26.6°$ and 54.8° corresponds to the (002) and (004) planes of the nano-graphite. With the introduction of Ru, no diffraction peaks of nano-graphite were shifted, and no diffraction peaks of RuO_2 were observed in the XRD patterns of RuO_2/nano-graphite. This result indicated that the content of RuO_2 too low to be detected by XRD or that amorphous phase RuO_2 existed, which was consistent with the XPS results.

3.3. Raman spectroscopy

To obtain further insight into the structure of the samples, the Raman spectra were measured and are shown in Fig. 5, which depicts the evolution of the peak value from nano-graphite to RuO_2/nano-graphite. The Raman spectrum of nano-graphite consisted of two peaks at 1426 cm^{-1} and

1660 cm^{-1}, which were assigned to the D peak and the G peak of graphite, respectively[26]. The D peak showed that there were some defects or impurity atoms in the atomic structure of nano-graphite, but it was also possible that fold and the edge effects existed on the nano-graphite surface. The clear strong peak near 1660 cm^{-1} belonged to the G sharp peak of nano-crystalline graphite, and was attributed to the E2g model vibration in the atomic planar layer of the graphite lattice [27].

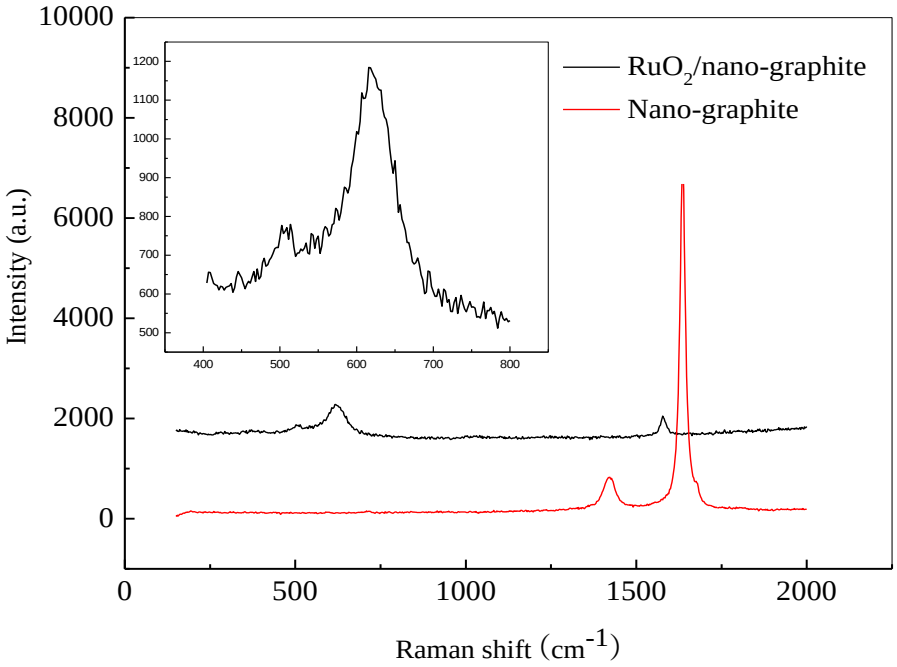

Figure 5. Raman spectra of nano-graphite and RuO_2/nano-graphite

With the introduction of ruthenium, the ruthenium characteristic peak at 625 cm^{-1} in the Raman spectroscopy of RuO_2/nano-graphite could be observed and the characteristic peak of nano-graphite disappeared. This result indicated that ruthenium oxide was successfully assembled on the surface of nano-graphite. The magnified Raman spectra in the inset of Fig. 5 showed that the two major Raman peaks corresponding to the ruthenium oxide crystalline (the A1g and B2g modes were located at 509 cm^{-1} and 625 cm^{-1}, respectively) [28]. The amorphous ruthenium oxide did not exhibit Raman peaks in the wavelength region of 100-2000 cm^{-1}, as shown in Fig. 5. [29]. It should be noted that the nano-crystalline ruthenium oxide particles with rutile structure could be prepared by the precipitation method. The results of XPS, XRD and Raman analysis, demonstrated that amorphous RuO_2 and crystalline RuO_2 co-existed in as-prepared RuO_2/nano-graphite.

3.4. AFM

As shown in Fig. 6, AFM was performed to determine the 3-dimensional surface images of nano-graphite and RuO_2/nano-graphite, as well as the distribution of RuO_2 on the nano-graphite flake.

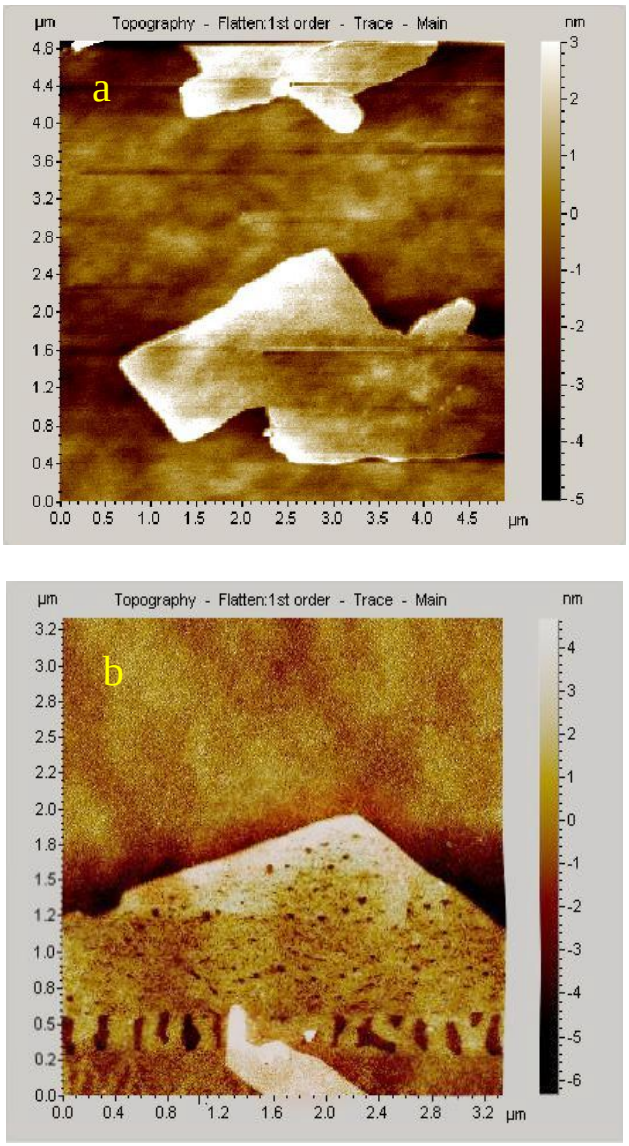

Figure 6. AFM images of (a) nano-graphite and (b)RuO_2/nano-graphite

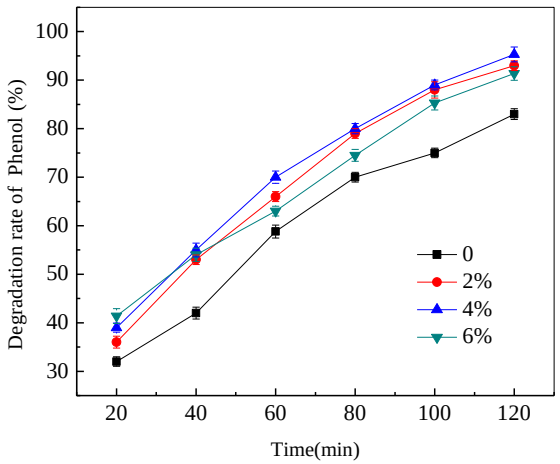

Figure 7. Influence of the RuO_2 content on phenol removal

Nano-graphite and RuO_2/nano-graphit in the laminated shape are shown in Fig. 6a and 6b, which was consistent with the SEM results. RuO_2 particles were also present across the nano-graphite sheet on the silicon substrate, leading to thin layers of RuO_2/nano-graphite (in Fig. 6b), which indicated the successful deposition of RuO_2 onto the surface of nano-graphite sheets [28]. Nano-graphite and RuO_2/nano-graphite samples revealed nanoscale structures with graphite sheet thickness of 2-3 nm and 3-4 nm, respectively.

3.5. Electrocatalytic performance evaluation of the cathode

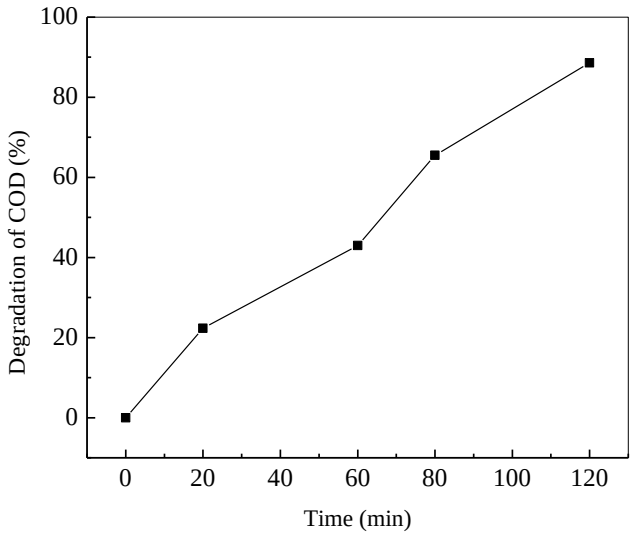

Figure 8. Removal of COD

The RuO_2/nano-graphite cathode was used for the electrocatalytic degradation of phenol, and the results are shown in Fig. 7. The removal rates of phenol with the RuO_2/nano-graphite electrode in the cathode compartment were larger than for the pure nano-graphite cathode. In Fig. 7, the largest removal rate was achieved using the RuO_2/nano-graphite cathode with 4% Ru content added. After 120 min electrolysis, the degradation rate of phenol reached 95.3% which was significantly higher than for the nano-graphite cathode (83.8%).

The removal of COD from simulated wastewater was studied by the electrocatalytic reaction in the RuO_2/nano-graphite cathode compartment. The result of COD removal is illustrated in Fig. 8. Half of the COD was removed within an hour. The electrocatalytic removal rate of the COD was up to 88.6% after 120 min when 4%-RuO_2/nano-graphite was used as the cathode.

3.6. The effect of RuO_2 on phenol removal at the RuO_2/nano-graphite cathode

In the terylene diaphragm cell, the removal of phenol in the cathode compartment was ascribed to indirect electrochemical oxidation. It is well known that the two-electron reduction of O_2 at the

graphite-cathode/water interface can generate H_2O_2; further, H_2O_2 can be converted to hydroxyl radicals (•OH). H_2O_2 and •OH are both powerful oxidants and could be used to degrade organic pollutants in the wastewater. To understand the degradation process in the RuO_2/nano-graphite cathode compartment, the concentration of H_2O_2 and the generation of •OH in situ during electrolysis were measured.

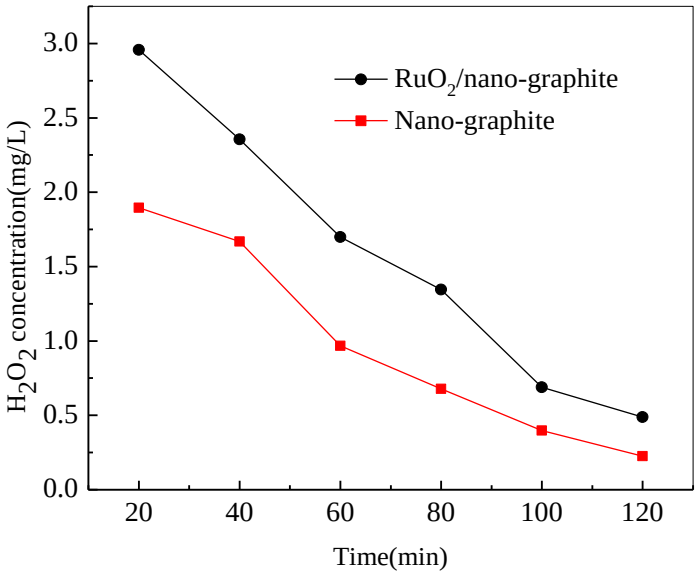

Figure 9. The concentration of hydrogen peroxide produced at nano-graphite and RuO_2/nano-graphite cathodes

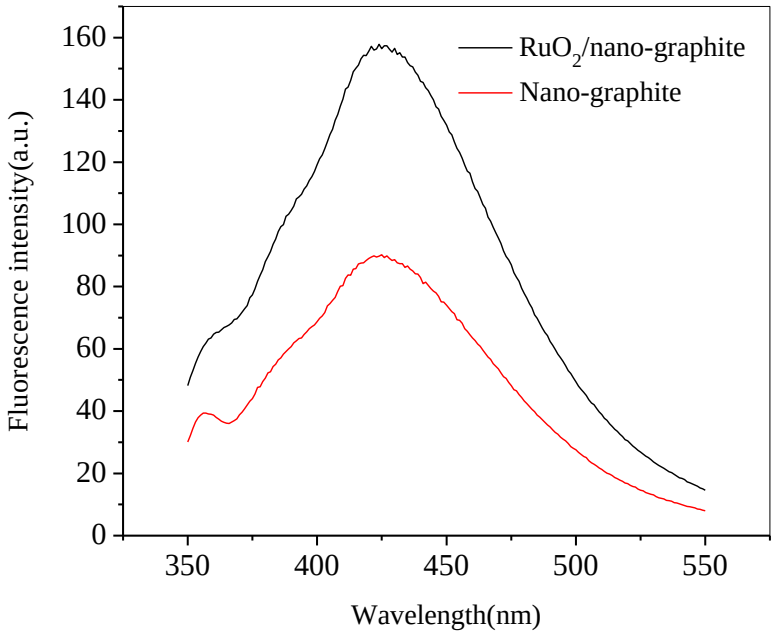

Figure 10. FL spectra changes of the nano-graphite and RuO_2/nano-graphite cathodes.

The concentration of H_2O_2 in the solution was determined by potassium permanganate titration. Fig. 9 shows that the behaviour of the two concentration curves for H_2O_2 were similar: the highest concentration of H_2O_2 occurred at the initial electrolysis, and the concentration of H_2O_2 decreased with prolonged electrolysis time. The concentration of H_2O_2 produced at the RuO_2/nano-graphite cathode was larger than at the nano-graphite cathode, perhaps because the RuO_2 catalyst accelerated the two-electron reduction of O_2 to H_2O_2 at the cathode.

Hydroxyl radical (•OH) has been proven to be a strong oxidant for the effective destruction of a large number of organic pollutants. Fig. 10 shows the yield of •OH from the cathodic chamber over the RuO_2/nano-graphite cathode and the nano-graphite cathode. The fluorescence (FL) intensity with the RuO_2/nano-graphite cathode was stronger than for the pure nano-graphite cathode under aeration conditions, indicating that the concentration of •OH radicals produced on the RuO_2/nano-graphite cathode was higher than for the pristine nano-graphite cathode, which was attributed to the activity of RuO_2 as a catalyst accelerating the decomposition of H_2O_2 to •OH.

The indirect catalytic degradation of phenol by RuO_2/nano-graphite was attributed to the products of the chemical or electrochemical reaction, depending on the RuO_2 properties.

One of the catalytic actions may be based on the electrical conductivity of RuO_2. The RuO_2 in the RuO_2/nano-graphite cathode can promote the generation of H_2O_2 and •OH via the reduction reaction of Ru^{4+} to Ru^{3+}, as follows [30]:

$$RuO_2 + H_2O + e^- \rightarrow RuO(OH) + OH^- \quad (1)$$

RuO(OH) is oxidized by O_2 as described by reaction (2).

$$2RuO(OH) + O_2 \rightarrow 2RuO_2 + H_2O_2 \quad (2)$$

Then, •OH radical is further produced by the decomposition of H_2O_2.

$$H_2O_2 \rightarrow 2\bullet OH \quad (3)$$

Another catalytic activity regarding the H_2O_2 and •OH production at the RuO_2/nano-graphite cathode may relate to the electronic properties of RuO_2. Oxygen molecules could first be adsorbed on RuO_2 via the d orbital hole of Ru, and then the O-O bond could be destroyed to form $RuO_2(O)$ [31], thereby further generating ·OH as shown in reactions (4) and (5).

$$2RuO_2 + O_2 \rightarrow 2RuO_2(O) \quad (4)$$

$$RuO_2(O) + H_2O \rightarrow RuO_2 + \bullet OH + OH^- \quad (5)$$

RuO_2 could easily adsorb oxygen molecules due to its high positive charge. In addition to its excellent electronic conductivity, comparable protonic conductivity and high chemical stability [32], this ability makes RuO_2 material promising as a durable cathode material.

4. CONCLUSION

The RuO_2/nano-graphite composite was synthetized through the chemical precipitation method, followed by calcination. Ruthenium was in the form of Ru^{4+}, and amorphous hydrous RuO_2 and crystalline state RuO_2 co-existed in the RuO_2/nano-graphite composite. The thicknesses of nano-graphite and RuO_2/nano-graphite were in the ranges of 2-3 nm and 3-4 nm, respectively. In addition, RuO_2/nano-graphite with 4% ruthenium presented the optimal electrocatalysis performance, such that

95.3% of phenol and 88.6% of COD can be degraded under 120 min electrolysis in the diaphragm electrolysis system in aeration conditions. Compared to the pure nano-graphite cathode, the RuO_2/nano-graphite cathode showed higher electrocatalytic performance, which was attributed to the the presence of RuO_2 producing more H_2O_2 and •OH to oxidize the phenol and cut down the COD in the wastewater. RuO_2/nano-graphite has a good prospect for application in the electrochemical catalytic degradation of organic pollutants in wastewater.

References

1. W. Xie, S. Yuan, X. Mao, W. Hu, P. Liao, M. Tong and A. N. Alshawabkeh, *Water Res.*, 47 (2013) 3573
2. L. Yue, J. Guo, J. Yang, J. Lian, X. Luo, X. Wang, K. Wang and L. Wang , *J. Ind. Eng. Chem.*, 20 (2014) 752.
3. E. Brillas and C. A. Martínez-Huitle, *Appl. Catal. B: Environ.*, 166-167 (2015) 603.
4. X. Yu and L. Qiang, *Advances in Materials Physics and Chemistry*, 2 (2012) 63.
5. L. Fan, Y. Zhou, W. Yang, G. Chen and F. Yang, *J. Hazard. Mater.*, 137 (2006)1182.
6. D. Chatterjee, B. Ruj and A. Mahata, *Catal. Commun.*, 2 (2001) 113.
7. H. Ma, X. Zhang, Q. Ma and B. Wang, *J. Hazard. Mater.*, 165 (2009) 475.
8. A. J. Méndez-Martínez, M. M. Dávila-Jiménez, O. Ornelas-Dávila, M. P. Elizalde-González, U. Arroyo-Abad, I. Sirés and E. Brillas,*Electrochim. Acta*, 59 (2012) 140.
9. X. Y. Duan, F. Ma, Z. X. Yuan, L. M. Chang and X. T. Jin, *J. Taiwan Institut. Chem. Eng.*, 44 (2013) 95.
10. C. R. Cost, C. M. R. Botta, E. L. G. Espindola and P. Olivi, *J. Hazard. Mater.*, 153 (2008) 616.
11. G. R. P. Malpass, D. W. Miwa, S. A. S. Machado and A. J. Motheo, *J. Hazard. Mater.*, 156 (2008) 170.
12. H. Wang. , Z. Y. Bian, G. Lu, L. Pang, Z. P. Zeng and D. Z. Sun, *Appl. Catal. B: Environ.*, 125 (2012) 449.
13. S. Irmak, H. I. Yavuz and O. Erbatur, *Appl. Catal. B: Environ.*, 63 (2006) 243.
14. E. Brillas, B. Boye, I. Sirés, J. A. Garrido, R. M. Rodríguez, C. Arias, P. L. Cabot and C. Comninellis, *Electrochim. Acta*, 49 (2004) 4487.
15. K. Hanna, S. Chiron and M. A. Oturan, *Water Res.*, 39 (2005) 2763.
16. A. Özcana, Y. Şahina, A. S. Koparalb and M. A. Oturanc, *J. Electroanal. Chem.*, 616 (2008) 71.
17. P. P. Jin, R. Chang, D. Q. Liu, K. Zhao, L. X. Zhang and Y. J. Ouyang, *Journal of Environmental Chemical Engineering*, 2 (2014) 1040.
18. Y. Y. Chu, Y. Qian, W. J. Wang and X. L. Deng, *J. Hazard. Mater.*, 199-200 (2012) 179.
19. J. L. Chen, J. Y. Wang, C. C. Wu and K. Y. Chiang, *Colloids Surf., A*, 379 (2011) 163.
20. X. J. Yu, T. Sun and J. F. Wan, *J. Nanosci. Nanotechnol.*, 14 (2014) 1.
21. D. Li, Z. P. Xing, X. J. Yu and X. W. Cheng,*Electrochim. Acta*, 170 (2015) 182.
22. K.S. Kim and N. Winograd, *J. Catal.*, 35 (1974) 66.
23. R. Awasthi and R. N. Singh, *Carbon*, 51 (2013) 282.
24. R. K. Raman, A. K. Shukla, A. Gayen, M. S. Hegde, K. R. Priolkar, P. R. Sarode and S. Emura, *J. Power Sources*, 157 (2006) 45.
25. Y. Liang, J. Li, Q. C. Xu, R. Z. Hu, J. D. Lin and D. W. Liao, *J. Alloys Compd.*, 465 (2008) 296.
26. K. N. Kudin, B. Ozbas, H. C. Schniepp, R. K. Prud'homme, I. A. Aksay and R. Car, *Nano Lett.*, 8 (2008) 36.
27. J. P. Tu, L. P. Zhu, K. Hou and S. Y. Guo, *Carbon*, 41 (2003) 1257.

28. C. Gómez-Navarro, R. T. Weitz, A. M. Bittner, M. Scolari, A. Mews, M. Burghard and K. Kern, *Nano Lett.*, 7 (2007) 3499.
29. J. Y. Kim, K. H. Kim, S. H. Park and K. B. Kim, Electrochim. Acta, 55 (2010) 8056.
30. H. F. Li, R. D. Wang and R. Cao, *Microporous Mesoporous Mater.*, 111 (2008) 32.
31. Y. J. Li, C. C. Chang and T. C. Wen, *J. Appl. Electrochem.*, 27 (1997) 227.
32. J. F. Shen, T. Li, W. S. Huang, Y. Long, N. Li and M. X. Ye, *Electrochim. Acta*, 95 (2013) 155.